CHANDRA
X-ray Center   60 Garden St., Cambridge Massachusetts 02138 USA

MEMORANDUM

Date: November 13, 2003
From: Richard J. Edgar
To: ACIS Team
Subject: Absolute QE of ACIS S2 and S3 from XRCF data at Oxygen K-α and Copper
            L-α
Cc: CXC Calibration Group
File: ACIS_QE_O_S23.tex
Version: 0.5

1   Abstract

The absolute quantum efficiency (QE) of ACIS chips S2 and S3 is derived at 0.525 keV (the oxygen K–α line) and 0.9297 keV (the copper L-α line) from flat field data taken at the X-Ray Calibration Facility (XRCF). The data were taken in May 1997. Absolute quantum efficienty is derived by comparing count rates of the ACIS chips (derived from high-speed tap data) and a Flow Proportional Counter (FPC) in the subject line. The FPC in question (fpc_hn) was calibrated absolutely at the synchrotron at BESSY.
The results are these:

	Oxygen	Copper
energy	0.5249 keV	0.9297 keV
	XRCF	
QE(S2)	0.228 ± 0.005	0.558 ± 0.014
QE(S3)	0.615 ± 0.013	0.841 ± 0.024
S3/S2	2.697 ± 0.0772	1.508 ± 0.0577
	CALDB	
QE(S2)	0.2120	0.5644
QE(S2)	0.5230	0.7861
S3/S2	2.467	1.3928
XRCF/CALDB	$1.093 \pm .0313$	1.083 ± 0.041
CALDB/XRCF	0.915 ± 0.026	0.9234 ± 0.035
ground correction r/y	0.900 ± 0.05	0.946 ± 0.05

The sense and size of this correction is approximately what is needed for consistency with grating measurements (Marshall, memo cited in text), and for some of the ACIS imaging mode observations of clusters of galaxies. The ground correction r/y in the table is based on memos by Marshall and by Butt & Spitzbart, and is explained in the text. It is directly comparable to the CALDB/XRCF ratio which results from this work.

2   Experimental Setup

During Phase I (as in eye, not Roman Numeral One) at XRCF, starting in early May 1997, the HRMA had been removed. The ACIS flight camera was placed at or near the former HRMA focal point, and flat-field tests were run at a variety of energies used earlier during the HRMA/ACIS calibration.

The HXDS (HRMA X-ray Detection System; i.e. ground calibration instruments) equipment in place included four Flow Proportional Counters (FPC) Beam Normalization Detectors (BND) near the front of the HRMA in the main chamber (the BND-H), and two detectors (one FPC and one high-purity Germanium Solid State Detector [SSD]) in Building 500, much closer to the source building up the beam pipe.

Two of the BND detectors (the fpc_hn, [the north BND-H], and the fpc_5, the FPC in building 500) were on translation stages, and could be moved around in the beam to test its uniformity. The former fpc_x2, the FPC used at the focal point of the HRMA during the HRMA-only testing (Phases C, D, and E) in Dec 1996 through February 1997, was placed in the fpc_hs (south BND-H) position.

Four of the HXDS detectors were calibrated were calibrated absolutely at BESSY in the summer and fall of 1997. These include the ssd_5, the ssd_x (focal point detector not used in the flat field tests), the fpc_hn and the fpc_x2 (during Phase I mounted in the fpc_hs position).

Since for the present analysis we are interested in the absolute low-energy calibration of the ACIS flight chips, we will use the calibrated HXDS detectors to determine the intensity and uniformity of the x-ray beam, and compare the count flux of ACIS to the photon flux predicted by the simultaneous BND measurements. These should differ by a factor of the ACIS QE.

The source used for this experiment was the Electron Impact Point Source (EIPS), using a SiO_2 anode mounted on a copper base. The source high voltage was set to approximately 1.7 keV, to avoid exciting the Si K$-\alpha$ line. The resulting spectrum has been shown by LETG measurements to contain the Oxygen K$-\alpha$ line at 0.525 keV, the Cu L$-\alpha$ complex near 0.9297 keV, a Bremmsstrahlung continuum, and a weak carbon K line which ACIS cannot see. Line energies are taken from Bearden (Rev Mod Phys, 39, 78, 1967).

Details of the HXDS calibration and beam uniformity test analysis can be found in the SAO report "XRCF Phase 1 Testing: Analysis Results," dated August 1999, and available on the web:

<div align="center">http://hea-www.harvard.edu/MST/simul/xrcf/report/index.html</div>

Of special interest are chapters 3 (HXDS Flow Proportional Counters) and 24 (EIPS Beam Uniformity).

The BND detectors were run continuously, and ACIS was run with the High Speed Tap (HST) attached to first one chip and then another. We will look at the S2 and S3 HST data for this initial analysis. The TRW_ID (test identifier) was changed whenever the HST was moved to another chip. The HXDS runid also changed at these times.

3   Analysis Procedure

3.1   Preparation of the ACIS data

The ACIS data were taken by the High Speed Tap, attached to one chip at a time. The full-frame data resulting from this were stored to disk (in the interests of space, they are archived on DLT tapes). Kenny Glotfelty then ran event finding software on them, producing FITS format event lists. These are still on the CfA disks, here:

<div align="center">/data/acis1/xrcf/PHASE_I/970509/I-IAS-EA-2.003</div>
<div align="center">/data/acis1/xrcf/PHASE_I/970509/I-IAS-EA-2.004</div>

These event lists are not quite in modern Level 0 format, so they were processed by grading and pulse height summing software (Dan Nguyen's `addfltgradeadu2subass` program) which was written to handle data in this format. In addition, the header keyword `ONTIME` must be copied to `LIVETIME`.

The ciao tool `dmextract` can then be used to extract spectra, either for a whole chip (which was done for S2), or selected areas (the S3 data were extracted one node at a time). These are made into xspec-compatible PHA files, which are histograms of number of events vs. pulse height in ADU. 4096

channels were used in these extractions.

The HXDS instruments produce as raw data products histogrammed pulse height spectra in ASCII files. These are summed by a perl script, since many iterations were performed during the time that ACIS was exposed in each case. The resulting summed spectra were then converted to minimal FITS files for fitting in xspec.

3.2 I-IAS-EA-2.003: the S2 test

Figure 1 shows the JMKmod fit to the S2 full-chip data. Included in the model are the oxygen K-α line at 0.525 keV, the copper L-α line, a Kramer continuum model, and the transmission of a beryllium filter of thickness 2 μm. The model was developed for the HPGe solid state detectors, with gain parameters altered for ACIS. Thus, instrumental edges will be those of germanium instead of silicon. This will impact continuum fits, but not line intensities, since we're interested in line counting rates (detected counts per second per area on the chip).

The fitting procedure does not involve a response matrix. The need of the xspec software to have such a data product is satisfied by feeding it a diagonal matrix. The convolution of source spectrum with instrument response is all done within the `JMKmod` software, which runs as a model subroutine to xspec.

The point of fitting the data with this model is to extract the flux in the line, by fitting and removing the flux in the nearby continuum. We believe this procedure can be accomplished to an accuracy of order 1%, even for much lower resolution instruments such as FPCs.

Figure 2 shows fits to the FPC pulse-height spectra of the same test. We will use only the fpc_hn for this analysis, since this counters was calibrated at BESSY. While the fpc_x2 was also calibrated at BESSY, the beam uniformity for this anode/filter combination was not measured along the line of sight to this detector. The relative quantum efficiency of the other FPCs at oxygen was established from this same flat field test, so the argument would be circular if we included them.

Note that while there are systematic residuals in the FPC fits near the oxygen line, the integral of the residuals (in the top, linear, plots) is near zero, so we believe the line flux is estimated accurately. The software does not represent the instrumental line shape in detail.

3.3 I-IAS-EA-2.004: the S3 test

In a similar way, Figure 3 shows the results of fitting one of four single-node extractions of the data from the S3 chip in test I-IAS-EA-2.004. Since the gains of the four nodes differ slightly, we found it easier to fit single-node spectra than all four nodes combined.

Figure 4 shows the fit to the fpc_hn data.

XRCF S2 Oxygen K−α HST event data
JMKmod fit: O−K, Cu−L, Kramer continuum

I−IAS−EA−2.003.pha

edgar 8−May−2003 09:59

XRCF S2 Oxygen K−α HST event data
JMKmod fit: O−K, Cu−L, Kramer continuum

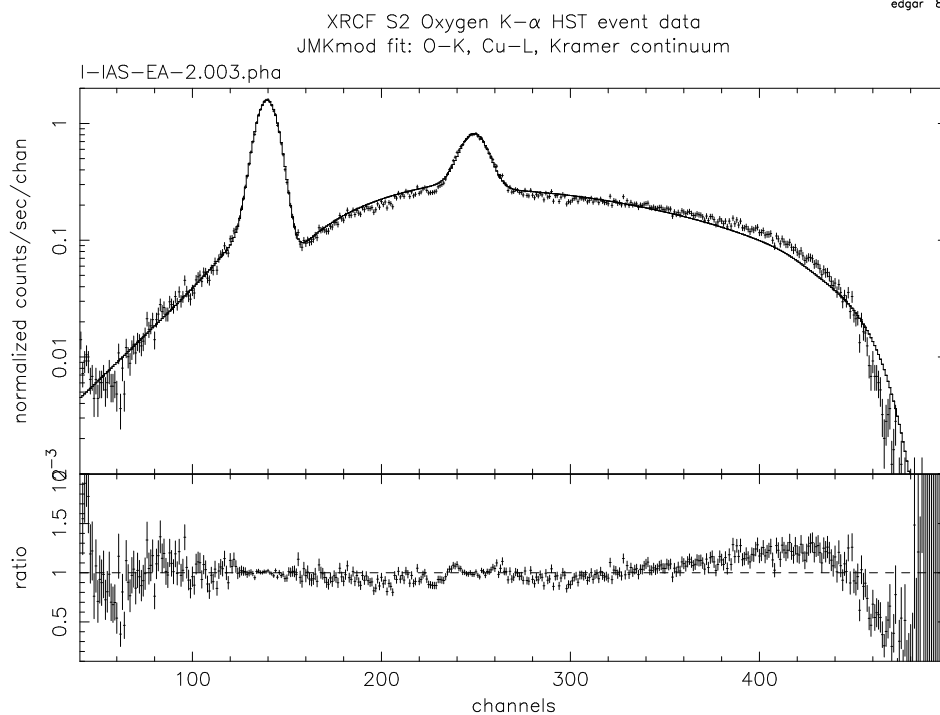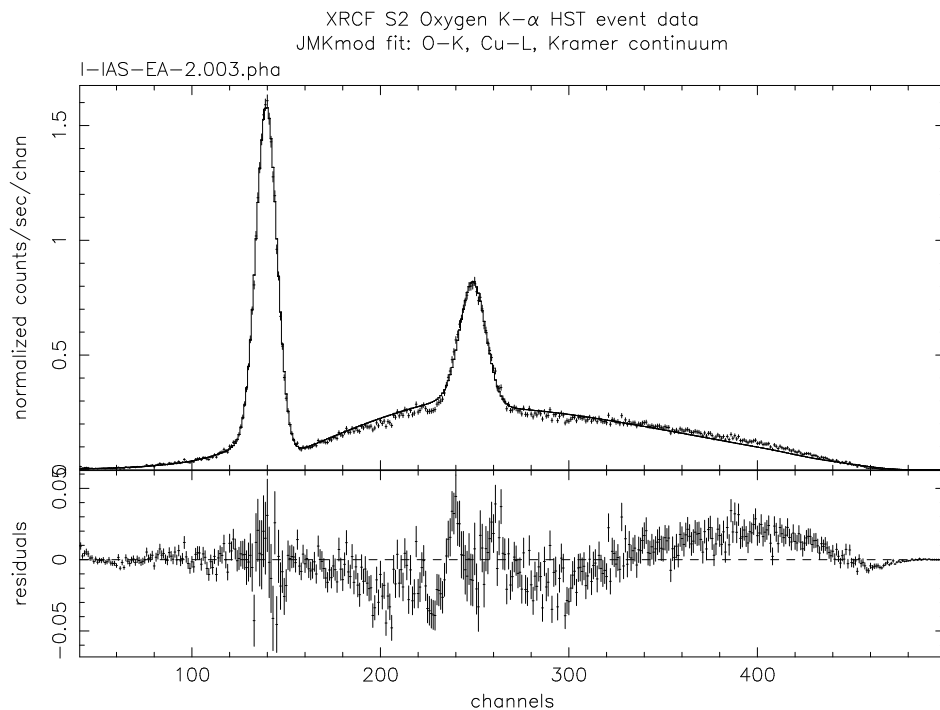I−IAS−EA−2.003.pha

edgar 8−May−2003 10:01

Figure 1: JMKmod fit to full-chip S2 data from I-IAS-EA-2.003
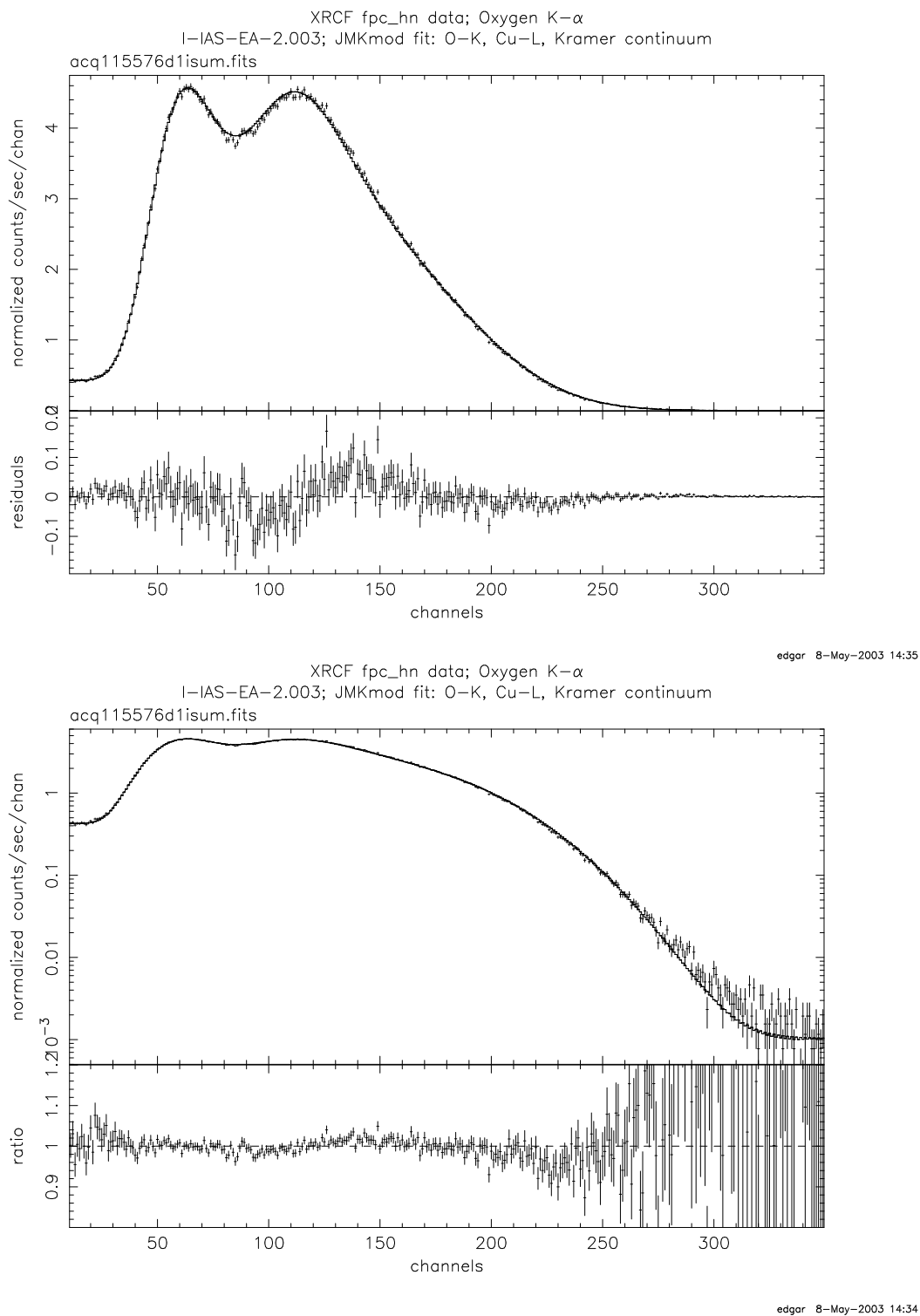
Figure 2: JMKmod fit to fpc_hn data from I-IAS-EA-2.003

XRCF S3c1 HST data; Oxygen K−α
JMKmod fit: O−K, Cu−L, Kramer continuum
I−IAS−EA−2.004_S3c1.pha

edgar 8−May−2003 10:05

XRCF S3c1 HST data; Oxygen K−α
JMKmod fit: O−K, Cu−L, Kramer continuum
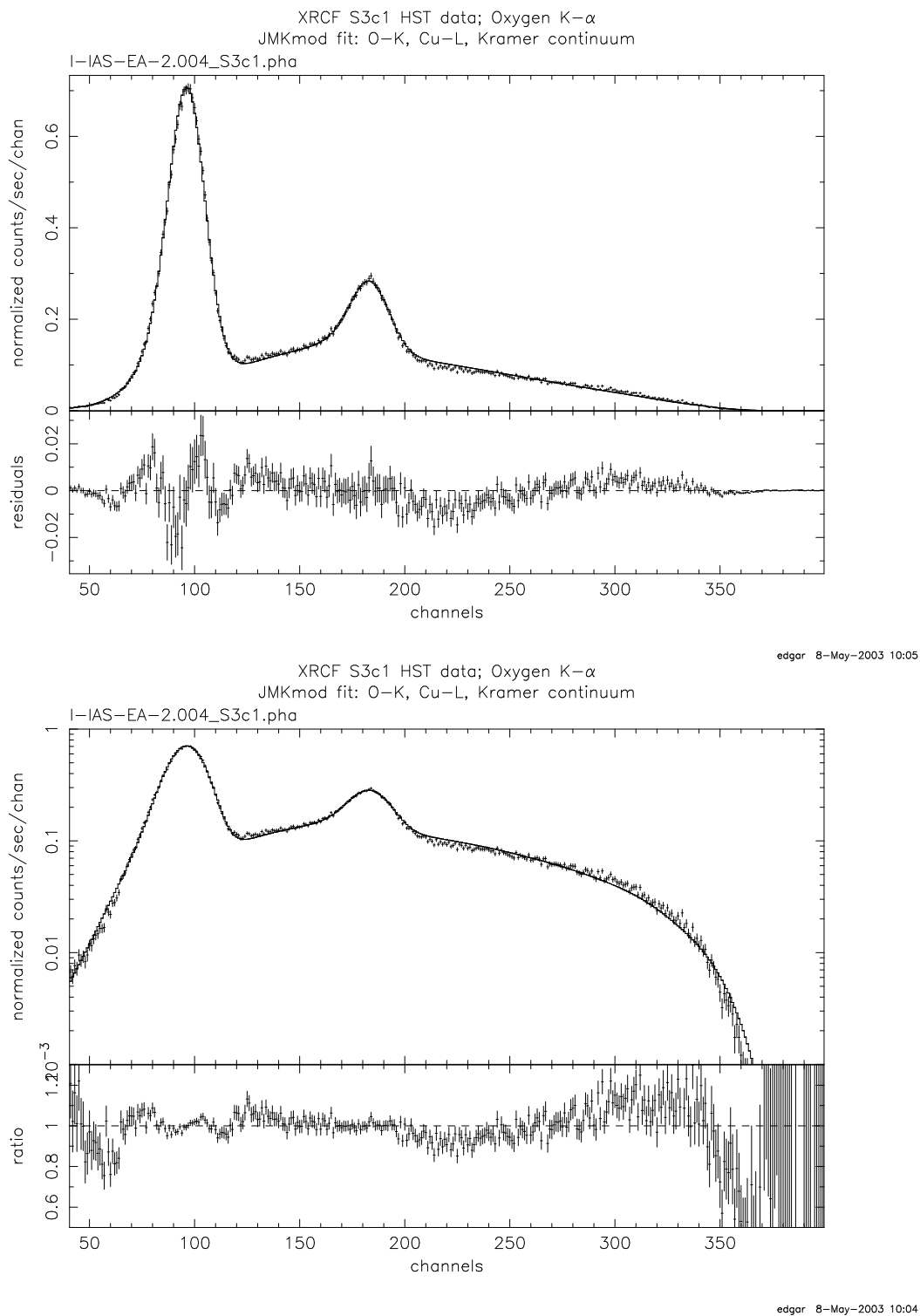I−IAS−EA−2.004_S3c1.pha

edgar 8−May−2003 10:04

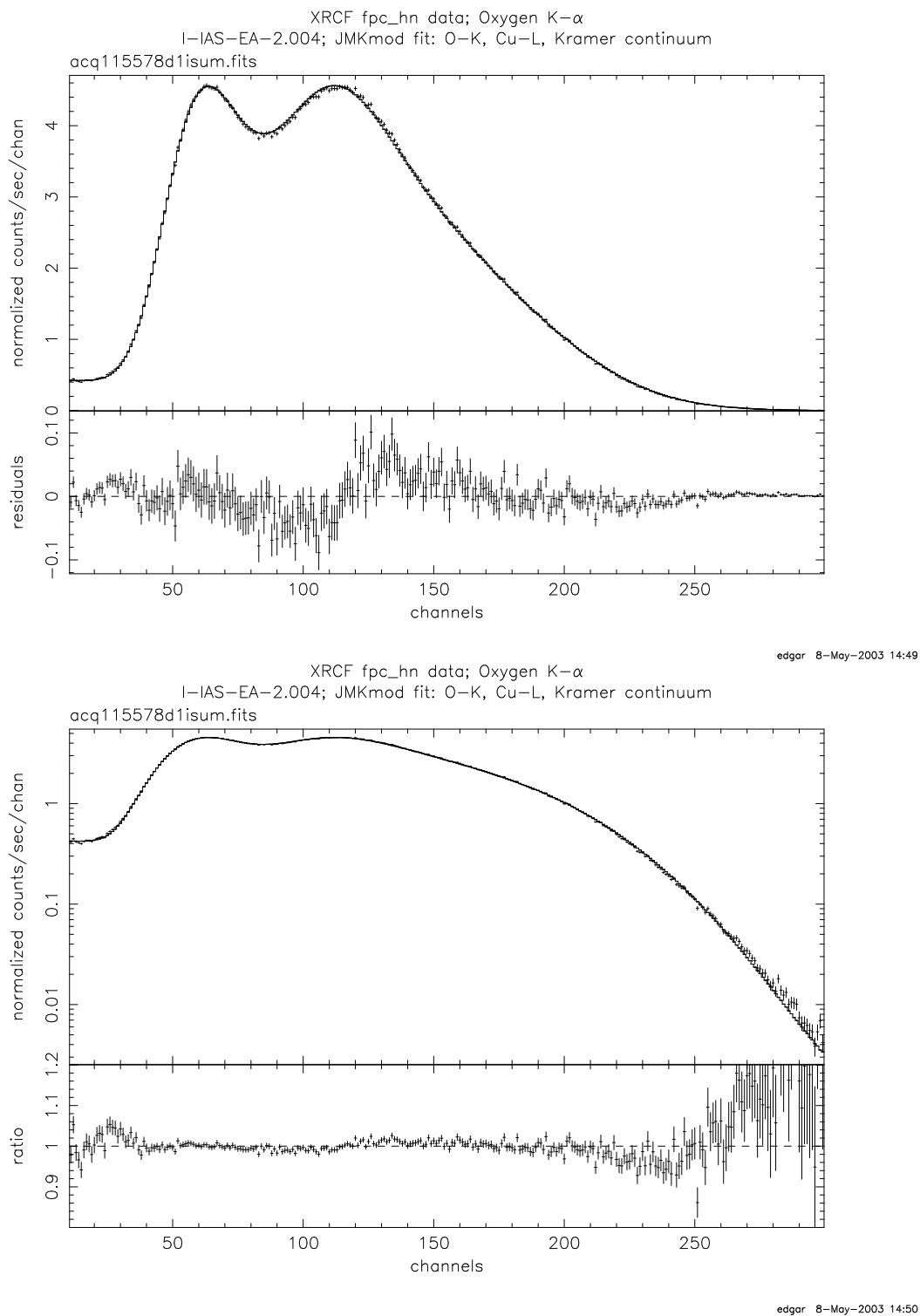Figure 3: JMKmod fit to single-node S3c1 data from I-IAS-EA-2.004

Figure 4: JMKmod fit to fpc_hn data from I-IAS-EA-2.004

3.4 Beam Uniformity

Another systematic effect may arise due to the non-homogeneity of the x-ray beam. This is controlled by mapping the relevant portions of the beam, using one or the other of the travelling BND detectors (the fpc_hn in the instrument chamber, and the fpc_5 in the pipe nearer the source). The test most relevant for this calculation has TRW_ID I-BND-BU-2.129. This is the only Beam Uniformity (BU) test done with the source in the same configuration (SiO_2 anode with Be filter and a source high voltage of about 1.7 keV). As it happens, it is nearly ideal for our purposes.

One iteration (spectrum with the HXDS equipment) is done with the fpc_hn along the line of sight between the source and each of the ten ACIS chips, and one final iteration is done with the fpc_hn in the parked position. If one were ordering a better test, one would also like a measurement at the fpc_x2 (i.e. fpc_hs) position, since that detector also has an absolute QE calibration.

We analyze the spectrum for each iteration for each of two detectors: fpc_hn and fpc_5. The fpc_5 flux is used to control for (possible) time-dependence of the source strength, while the fpc_hn is moved around as specified above.

The BU factor is defined to be the ratio of count fluxes C_{hn}/C_5. The absolute scale of these ratios is unimportant, as geometrical factors will cancel, since only ratios of these BU factors appear in the final product.

In the event, we find that this test shows the beam is (within about 1% error bars) flat. The RMS deviation between iterations is essentially the same as the random errors in each.

4 Results

We proceed to give the results. Let the countrate for a detector be C_{det} in units of cts s^{-1}. Each detector has an area, A_{det} in cm^2, a source distance d_{det} in cm. In addition, each detector has an energy-dependent quantum efficiency, QE_{det}, which I find it useful to think of in units of cts photon^{-1}. For the BND detectors, these are taken from the BESSY calibration, as reported in table 3.10 of the MST report *XRCF Phase 1 Testing: Analysis Results*. The QE of the ACIS chips is, of course, the goal of the present analysis. Furthermore, there is a beam uniformity correction for each detector position, BU_{det}.

For each detector then, the source luminosity is given by:

$$S = \frac{C_{det}}{A_{det} QE_{det}} \times d_{det}^2 BU_{det}$$

Since all detectors are looking at the same source at the same time, S is independent of the detector. Setting the two measurements of S equal, and solving for QE_{ACIS}, we obtain:

$$QE_{ACIS} = QE_{hn} \times \frac{C_{ACIS}}{C_{hn}} \times \frac{A_{hn}}{A_{ACIS}} \times \frac{BU_{ACIS}}{BU_{hn}} \times \frac{d_{ACIS}^2}{d_{hn}^2}$$

The ACIS area is taken from the POG, version 5.0, table 6.1, which gives the pixel size as 24.0 microns. This is for the flight temperature, $-120°$C, while the XRCF measurements were done at $-110°$C. I neglect the thermal expansion. Each node is 256×1024 pixels, minus the edge rows and columns. This gives a total of 259,488 pixels, for a total area of 1.4952 cm^2 per node, or 5.9809 cm^2 for a whole chip.

We give contributing quantities and final results in tables 1 and 2. We also plot the CALBD QE curves for both S2 and S3, and our derived results in Fig 5.

One possible systematic effect we have neglected here concerns the finite width of fluorescent lines in electron impact sources, especially for low$-Z$ elements such as oxygen. However, the LETG calibration

Field	S2	S3	units
TRW_ID	I−IAS−EA−2.003	I−IAS−EA−2.004	...
energy	0.5249	0.5249	keV
C_hn	138.4	137.0	cts s^{-2}
err_C_hn	.4282	0.28	cts s^{-2}
ap_area_hn	32.24	32.24	cm^2
ap_hn_err	0.16	0.16	cm^2
d_factor_hn	.9503	.9503	...
QE_hn	0.2251	0.2251	...
QE_hn_err	0.0018	0.0018	...
F_hn	18.12	17.94	ph cm^{-2} s^{-2}
err_F_hn	0.35	0.37	ph cm^{-2} s^{-2}
C_acis	24.70	65.95	cts s^{-2}
err_C_acis	.11	.11	cts s^{-2}
BU	0.1224	0.1206	...
BU_err	0.0012	0.0016	...
BU_hn	0.1210	0.1210	...
BU_hn_err	0.0016	0.0016	...
QE_caldb	0.2120	0.5230	...
QE_acis	0.2279	0.6147	...
QE_err	0.0045	0.0128	...

Table 1: Raw and derived quantities leading to the computation of the ACIS S2 and S3 QE at oxygen K−α.

included a measurement of the width of this line under slightly different circumstances (filter, high voltage) from this same source. They find that the flux in the line is down by more than two orders of magnitude before we get to the energy where the resonant absorption in the filter (and oxide layer on the CCD) occur near 0.53 keV. We therefore believe we are justified in neglecting this effect.

5 Placing these results in context

Based on observations with ACIS and both of the gratings (LETG and HETG), Herman Marshall has put together a memo, "Preliminary Results Concerning Calibration of the *Chandra* LETG/ACIS Effective Area," dated may 13, 2002, and available here:

http://space.mit.edu/ASC/calib/letg_acis/letg_acis_cal.ps.gz

In this memo he compares lines observed with the gratings in positive and negative orders, and derives ratios of the QE for FI and BI chips. He finds that, while FI/FI ratios and BI/BI ratios are all consistent with unity, a (wavelength dependent) correction of -10–15% is required to the FI/BI QE ratio, as compared to the CALDB QE numbers.

This correction is partly due to an unmodeled effect of cosmic rays on the quantum efficiency. Yousaf Butt and Brad Spitzbart have released a memo "ACIS Cosmic Ray Induced Dead Area," available here (on the internal CfA HEAD network):

/data/acis28/ybutt/CR_DEAD/CR_DEAD_memo1.pdf

The effect is that cosmic ray hits on the FI chips tend to make large blooms, involving typically 500 pixels above the split threshold. Any event landing on or ajacent to these blooms will be misgraded by the flight software, and either discarded on board or neglected in analysis. This represents a decrement

Field	S2	S3	units
TRW_ID	I−IAS−EA−2.003	I−IAS−EA−2.004	...
energy	0.9297	0.9297	keV
C_hn	64.73	65.8489	cts s^{-2}
err_C_hn	.7994	0.1788	cts s^{-2}
ap_area_hn	32.24	32.24	cm^2
ap_hn_err	0.16	0.16	cm^2
d_factor_hn	.9503	.9503	...
QE_hn	0.5925	0.5925	...
QE_hn_err	0.0054	0.0054	...
F_hn	3.22	3.28	ph cm^{-2} s^{-2}
err_F_hn	0.07	0.06	ph cm^{-2} s^{-2}
C_acis	10.7420	16.4819	cts s^{-2}
err_C_acis	.1144	.348	cts s^{-2}
BU	0.1216	0.1164	...
BU_err	0.0012	0.0012	...
BU_hn	0.1148	0.1148	...
BU_hn_err	0.0015	0.0015	...
QE_caldb	0.5644	0.7861	...
QE_acis	0.5577	0.8412	...
QE_err	0.0141	0.0242	...

Table 2: Raw and derived quantities leading to the computation of the ACIS S2 and S3 QE at copper L−α.

to the quantum efficiency. The effect is estimated at $3.68 \pm 0.21\%$ for grade 0 events on the FI chips. It should be very nearly energy independent, and, it is thought, of similar magnitude for other "good" grade events.

The analysis has not been carried out for BI chips, though a visual inspection of raw-mode frames indicates the effect is approximately an order of magnitude less than for the FI chips, $\sim 0.29\%$. We neglect this effect for BI chips in the following analysis.

Clearly this correction would apply only to flight data.

Marshall defines a correction factor

$$r(\lambda) \equiv \frac{(QE_{FI}/QE_{BI})_{true}}{(QE_{FI}/QE_{BI})_{caldb}}$$

which he derives from flight data. Since he is comparing to FI chips affected by the cosmic ray bloom effect, this factor r already contains a factor of $y \equiv 1 - 0.0368$.

The appropriate correction for ground-based data (which suffers much less from cosmic ray blooms) would then be r/y if applied to a FI chip, or y/r if applied to a BI chip. Since the above results show that the QE of the BI chips seems to be underestimated, we apply this correction to the S3 QE curve, for comparison. Note that the factor r is typically known only to an accuracy of about $\pm 5\%$ (and worse at longer wavelengths).

If we take the above definition of r, and presume that $(QE_{FI})_{true} = y\,(QE_{FI})_{caldb}$, it follows that

$$(QE_{BI})_{true} = y/r\,(QE_{BI})_{caldb}.$$

The results are plotted in Fig. 6. As can be seen, the measured QE values at Cu L−α are consistent with the notion that the CALDB is correct for S2 and underestimated by factor y/r for S3. At O K−α,
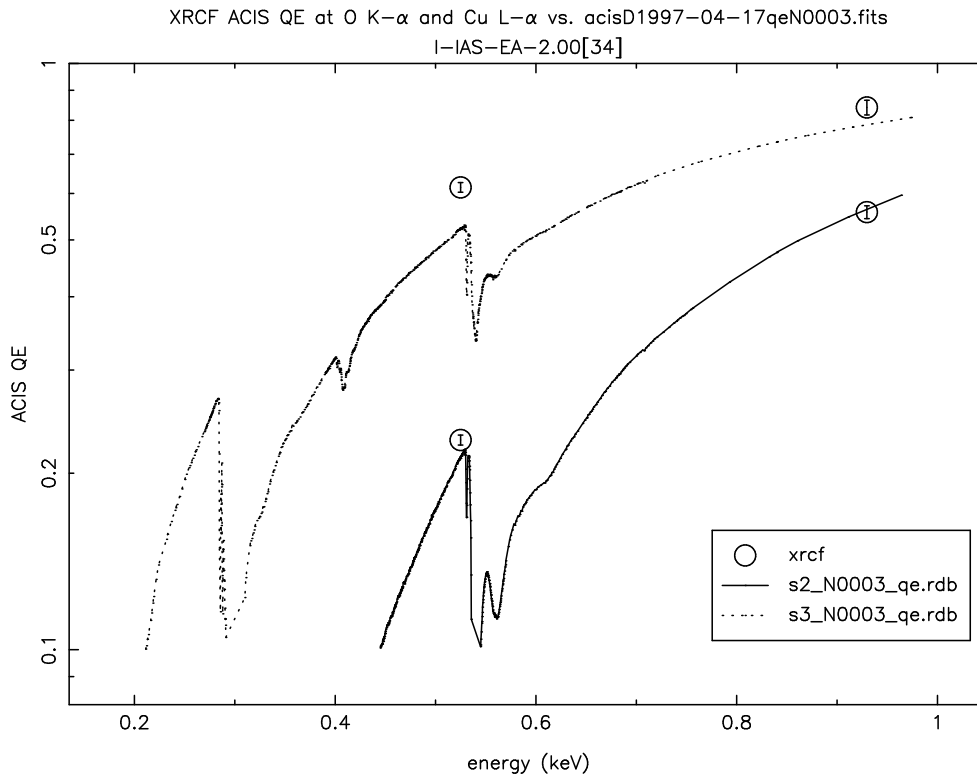
Figure 5: Derived QE of S3 and S2 at oxygen K–α and copper L–α. Also plotted are the released CALDB products from file `acisD1997_04_17qeN0003.fits`

the situation is a bit more murky. It looks as if both QE measurements may be a bit high relative to the above scenario. We will examine our analysis for other systematic effects.

It also seems clear that the empirical r correction curve from Marshall should be revisited from physical reasoning, now that we know where to look. In particular, the extrapolation to low energy is difficult due to the quality of the available data. The ratio r is consistent (within large error bars) with unity at low energies (long wavelengths), but this may not in fact be an accurate representation of the instrument response. A recent LETG-ACIS observation of Mrk 421 in outburst may provide the capability to extend the measurement of r to lower energies with greater confidence.

The conclusion to be drawn would seem to be that the flight FI QE should be decremented by factor $y = 0.9632$, and the flight BI QE should be increased by a factor consistent with y/r.

6   Future Work

There exist flatfield measurements using an iron anode that produce a comples of iron L lines (plus oxygen K). Analysis of these data will be complicated by the presence of at least 3 lines in the spectrum, which cannot be resolved by the FPC detectors. However, if approximate ratios can be fixed from grating data, or from the ACIS data themselves, a reasonable estimate of the ACIS QE can be derived at this energy (0.706 keV).

Analysis of some higher energy data, to show that the correction r goes to y at high energies, as required by cluster data, would also be useful.

In addition, we have data on the BI chips only at carbon K–α, which will be useful in the extrapolation of the QE curve to the lowest ACIS energies.

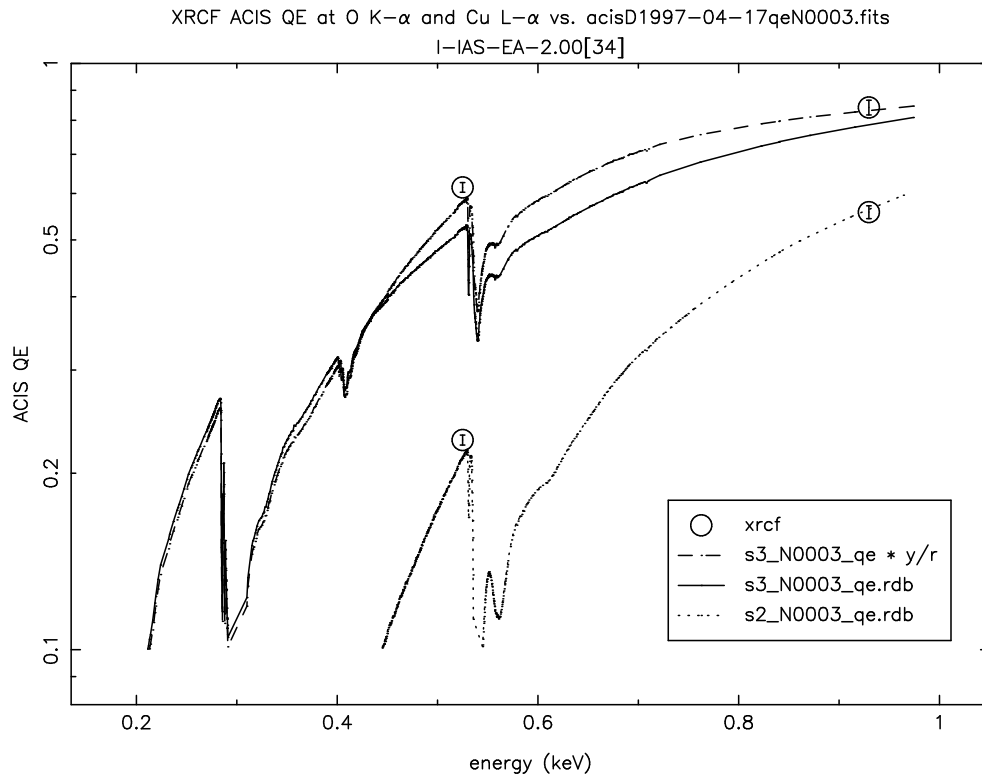XRCF ACIS QE at O K–α and Cu L–α vs. acisD1997–04–17qeN0003.fits

I–IAS–EA–2.00[34]

Figure 6: Derived QE of S3 and S2 at oxygen K–α and copper L–α. Also plotted are the released CALDB products from file `acisD1997_04_17qeN0003.fits`, and the corrected S3 quantum efficency curve, $y/r\ QE_{S3}$ The correction factors are r, Marshall's empirical grating correction, and y, the flight FI decrement due to cosmic ray dead area (see text).

The model QE of the ACIS chips and/or the OBF can then be re-fit using these absolute measurements as constraints.

There are also high-speed tap data for other chips at these same energies, so that the I-array chips can be checked. This will also allow comparison of the model x-ray transmissions of the two optical blocking filters (on the I- and S-array).